Journal of Materials Chemistry C

# Photophysical, Electrochemical and Solid State Properties of Diketopyrrolopyrrole based Molecular Materials: Importance of Donor Group



| | |
|---|---|
| Journal: | *Journal of Materials Chemistry C* |
| Manuscript ID: | TC-ART-11-2013-032251.R2 |
| Article Type: | Paper |
| Date Submitted by the Author: | 25-Jan-2014 |
| Complete List of Authors: | Patil, Satish; Indian Institute of Science, Solid State and Structural Chemistry Unit<br>Nutalapati, Venkatramaiah; Indian Institute of Science, SSCU<br>Dhar, Joydeep; Indian Institute of Science, SSCU<br>A, Anitha; Indian Institute of Science, SSCU |
| | |

# Photophysical, Electrochemical and Solid State Properties of Diketopyrrolopyrrole based Molecular Materials: Importance of Donor Group

Joydeep Dhar, N. Venkatramaiah, Anitha A and Satish Patil*

Solid State and Structural Chemistry Unit, Indian Institute of Science, Bangalore 560012

* To whom correspondence should be addressed

Dr. Satish Patil
Tel: +91-80- 22932651
Fax: +91-80-23601310
E-mail: satish@sscu.iisc.ernet.in

**Abstract**

Diketopyrrolopyrrole (DPP) based molecular semiconductors have emerged as promising materials for high performance active layer in organic solar cells. It is imperative to comprehend the origin of such property by investigating fundamental structure property correlation. In this report, we have investigated the role of donor group in DPP based donor-acceptor-donor (D-A-D) structure to govern the solid state, photophysical and electrochemical properties. We have prepared three derivatives of DPP with varying strength of donor groups such as phenyl (PDPP-Hex), thiophene (TDPP-Hex) and selenophene (SeDPP-Hex). The influence of the donor units on the solid state packing were studied by single crystal X-ray diffraction. The photophysical, electrochemical and density functional theory (DFT) results were combined to elucidate structural and electronic properties of three DPP derivatives. We have found that, these DPP derivatives crystallized in monoclinic space group $P2_1/c$ and show herringbone packing in the crystal lattice. The derivatives exhibit weak π-π stacking interactions as two neighboring molecules are slipped away from each other with varied torsional angle at donor units. The high torsional angle of 32° (PDPP-Hex) between phenyl and lactam ring results weak intramolecular interaction between donor and acceptor while TDPP-Hex and SeDPP-Hex show a lower torsional angle of 9° and 12° with strong overlap between donor and acceptor units. The photophysical properties reveal that PDPP-Hex exhibits high Stokes shift of 0.32 eV and SeDPP-Hex shows high molar absorption co-efficient of 33600 L $mol^{-1}cm^{-1}$ with low band gap of ~2.2 eV. The electrochemical studies of SeDPP-Hex indicate pronounced effect of selenium in stabilizing the LUMO energy levels and this further emphasizes the importance of chalcogens in developing new *n*-type organic semiconductors for optoelectronic devices.

## 1. Introduction

In the past decade, the performance of optoelectronic devices based on donor-acceptor (D-A) π-conjugated materials has been remarkably improved and such materials represent as promising candidates for flexible electronic devices.[1-4] Recently, tremendous efforts have been devoted to develop low band gap materials based on the concept of D-A approach.[5-7] The materials with the combination of donor (D) and acceptor (A) moieties exhibit narrow optical band gap with intramolecular charge transfer (ICT) character leading to unique properties such as efficient light harvesting in solar spectrum and high charge carrier mobility in organic field effect transistors (OFETs).[8-10] It is well established in literature that, the performance of the electronic devices strongly depends on the molecular packing of donor-acceptor, purity and type of electrodes.[11-13] The donor and acceptor materials have undergone significant diversification over a period of time. Different symmetrical D–A–D or A–D–A, or even more complex combinations such as linear ADADA, DADAD or three-fold symmetry have led power conversion efficiencies in the range of 3–6% in organic solar cells.[2, 3, 14-16]

In this regard, diketopyrrolopyrrole (DPP) unit has been extensively used as an acceptor to synthesize D-A based low band gap conjugated polymers and small molecules.[17, 18] The excellent thermal and photostability, planarity of the chromophore, easier structural modification and ambipolar charge carrier transport make DPP based molecule an ideal choice for optoelectronic device applications.[19, 20] Careful introduction of electron donating or withdrawing groups on lactam ring leads to novel low band gap materials by tuning its highest occupied molecular orbitals (HOMO) and lowest unoccupied molecular orbitals (LUMO) energy levels which determine the electronic properties and device performances.[21, 22] Recently, Yang and co-workers have reported power conversion efficiency (PCE) of 9.5% using DPP based polymer in tandem solar cells.[23] Rene Janssen group has demonstrated systematic enhancement of PCE of organic solar cells up to 9.6% with increase in the number of DPP based active layers in tandem cell configuration.[24] In organic thin film transistor (OTFT), the favorable intermolecular solid state aggregation of the DPP leads to highly efficient organic semiconductors with high charge carrier mobilities exceeding the corresponding value of amorphous silicon.[9, 25-27] For the past three years, our group has been actively involved in development and investigation of structure–property relationship of several DPP based D-A-D small molecules and conjugated polymers.[28,

[29] Recently, we have reported an informative study on single crystal X-ray analysis of functionalized DPP with varied alkyl and alkoxy chains. The study reveals that DPP derivatives with linear alkyl chains exhibit efficient π-π stacking pattern leading to effective solid state packing.[30] In parallel effort, other leading research groups have developed DPP-based materials with different types of donor groups such as phenyl, thiophene and furan rings.[23, 31-37] These heterocyclic rings were covalently linked with lactam ring at 3 and 6 positions of DPP unit to open up the avenue of multitude of D-A combinations to further optimize the electronic properties.[38] It is well documented that the replacement of phenyl with thiophene unit enhances the co-planarity of DPP unit for efficient π-π stacking.[20] Different types of derivatives encompassed with thiophene and thiophene based heterocycles as π-spacer exhibit most promising D-A structure in connivance with the DPP core.[18, 39, 40] Bijleveld and co-workers have reported two different co-polymers varied with thiophene and furan unit and revealed that both the materials exhibit similar hole mobilities in OFET.[41] The structure-property and device performances of thiophene-based DPP materials have been widely investigated, but the fundamental questions concerning the solid state and photophysical properties remain unanswered for selenophene-based DPP.[23, 42, 43] Since the aromatic resonance energy follow the order of phenyl (1.56 eV) > thiophene (1.26 eV) > selenophene (1.25 eV), the enhancement of the donating strength would lead to greater quinoidal character of the donor-acceptor bond predicting to enhance the planarity and effective conjugation length and would reduce the band gap of the organic semiconductors.[44] Moreover the beneficial influence of selenium e.g. easier polarisability to accommodate greater charge, strong intermolecular Se···Se interaction leading to improved inter chain charge transfer, and lower ionization potential conducive to reduce the band gap.[45, 46] In Se···Se interaction, the lone pair in an occupied 'p' orbital of selenium atom interacts with the empty Se-C $\sigma^*$ orbital of neighbouring selenium, together with induction and dispersion forces.[47] Introduction of selenophene as donor in DPP based architectures and to compare its molecular arrangements with other donors would be interesting to study the fundamental structure–property correlation. Motivated by these questions, we have synthesized three DPP based small molecules with different donor groups such as phenyl, thiophene and selenophene in D-A-D architecture to understand the effect of donor unit on the solid state packing arrangements and its influence on the photophysical and electrochemical properties. The bigger size of selenium (van der Waal radius, r= 1.9 Å) with higher polarisability (3.8 $Å^3$) and lower ionization

potential (9.75 eV) as compared to sulfur (10.36 eV) renders overall system worthy to investigate with respect to their solid state packing and photophysical properties.

## 2. Experimental Section

**Materials:** *t*-BuOK was received from Sigma-Aldrich. *N*-methyl-2-pyrrolidone (NMP), dimethyl formamide (DMF), hexane, and ethyl acetate of analytical grade were purchased from S.D. fine chemicals. Potassium carbonate ($K_2CO_3$) and 1-bromohexane were supplied by Spectrochem. All the chemicals were used as received without any further purification.

**2.1 Synthesis:** The derivatives of DPP (PDPP-Hex, TDPP-Hex, and SeDPP-Hex) were synthesized according to the reported procedure in the literature.[35, 36, 48] *N*-alkylation was carried out as shown in Scheme 1. After the alkylation, the final products were characterized by $^{1}H$, $^{13}C$ NMR, elemental analysis and ESI-MS spectroscopy. The detailed synthetic protocol and characterization is given in supporting information.

### 2.2 Characterization

The $^{1}H$ NMR spectra were recorded in Bruker Avance NMR spectrometer at 400 MHz frequency. $CDCl_3$ and TMS were used as solvent and internal standard, respectively. Elemental analysis of DPP molecules was carried out in Thermo Finningan Flash EA 1112 CHNS analyzer. Mass analysis was performed in Thermo LCQ Deca XP MAX instrument by electrospray ionization technique. The optical absorption spectra of three DPP molecules were recorded in toluene with Perkin-Elmer (Lambda 35) spectrometer at room temperature. Steady state emission spectra of DPP derivatives were monitored in Horiba JobinYvon Fluorolog3 fluorometer and quantum yields were determined using integrated sphere. Time resolved fluorescence decay measurements were carried out with time correlated single photon counting (TCSPC) method. Transmission Electron Microscopy (TEM) images were taken in Zeol field emission microscope at 200 kV at room temperature. The structural properties of the vacuum sublimed thin films of DPP derivatives were investigated by Philips X-pert diffractometer with Cu Kα ($\lambda$ = 1.5418 Å) radiation. Differential scanning calorimetry (DSC) analysis was carried out in Mettler Toledo DSC1 STARe system (chiller cooled) with $N_2$ flow of 40 mL/min with an empty Al pan taken as standard. All samples were heated with a heating rate of 10 °C/min. Redox properties of three DPP derivatives were evaluated by cyclic voltammetry experiment (CH electrochemical

analyzer). Ag/AgCl was used as reference electrode whereas Pt was employed as both working and counter electrodes. Dry chloroform and tetrabutylammonium hexafluorophosphate were used as solvent and supporting electrolyte. Ferrocene/ferrocenium ($Fc/Fc^+$) couple was used as standard electrochemical reference. The energies of HOMO and LUMO and corresponding band gap were calculated from the oxidation and reduction potential. The position of HOMO and LUMO were computed from the equation **1** and band gap was determined from the difference between them.

$$HOMO = -(E_{ox} + 4.5)\ eV;\ \ LUMO = -(E_{red} + 4.5)\ eV \qquad (1)$$

### 2.3 Single Crystal X-ray Diffraction

Single crystal X-ray diffraction data sets were collected on an Oxford Xcalibur (Mova) diffractometer equipped with an EOS CCD detector using MoKα radiation (λ = 0.71073 Å). The crystals were maintained at 110 K during data collection using the cryojet-HT controller. All structures were solved by direct methods using SHELXS-97 and refined against $F^2$ using SHELXL-97. H atoms were located geometrically and refined isotropically. The WinGX package was used for refinement and production of data tables and ORTEP-3 for structure visualization and making the molecular representations. Analysis of the H-bond and π···π interactions were carried out using PLATON for all the structures. Packing diagrams were generated using MERCURY.

## 3. Results and Discussions

The DPP derivatives with different donor units at 3 and 6 positions were prepared by using aryl or hetero-aryl carbonitrile (Ar-CN) and succinic acid ester as shown in Scheme 1. PDPP was prepared according to the established synthetic methodology.[48] The presence of phenyl rings at 3 and 6 positions on DPP core enhances repulsive interaction with adjacent lactam ring, resulting in a twisted molecular geometry. However, this twisted geometry can be alleviated by introducing five membered heterocyclic units on DPP to attain highly co-planar molecular backbone for efficient π-π stacking. To compare the molecular arrangements and rationalize the photophysical properties, we have prepared DPP derivatives with thiophene and selenophene units. TDPP was synthesized as reported in literature whereas selenophene-2-carbonitrile was prepared by one pot synthesis as described by Lohaus.[49] Reaction of selenophene-2-carbonitrile

with diethyl succinate in presence of sodium afforded the selenophene substituted DPP. The obtained DPP derivatives were deep red in color with low solubility due to very strong intermolecular interaction between N-H and C=O groups. In order to ensure good solubility of the resultant DPP derivatives, alkyl chains were introduced on nitrogen atoms of DPP unit with 1-bromohexane in presence of NMP and DMF (2:1 ratio) for PDPP-Hex and in DMF for TDPP-Hex and SeDPP-Hex at 125 °C to have desired final products with good yield. The obtained three DPP derivatives were characterized by $^{1}H$, $^{13}C$ NMR and ESI-MS spectroscopy (supporting information, Figure S1, S2, S3 and S4, ESI†).

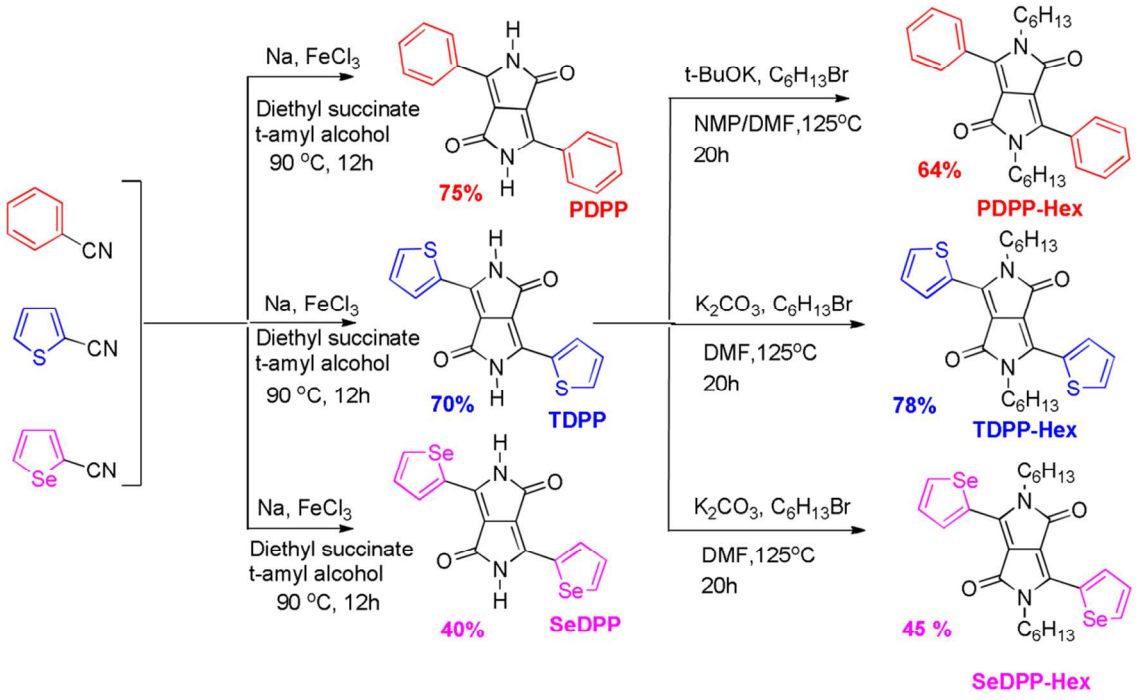


**Scheme 1:** Synthesis of DPP derivatives with varied donor units.

### 3.1 Photophysical properties

All three DPP molecules exhibit dual band absorption spectra which is a characteristic feature of the D-A-D based derivatives.[6] The high energy band corresponds to π→π* transition whereas the origin of low energy band is due to the intramolecular interaction between donor and acceptor moiety. We have observed three striking features in the absorption spectra (Figure 1a) of these derivatives. Firstly, we have observed a gradual bathochromic shift of both π→π* and low energy band on going from PDPP-Hex to TDPP-Hex to SeDPP-Hex, indicating the decrease in

band gap with inclusion of thiophene and selenophene as donor groups. The lowest optical band gap was observed for SeDPP-Hex in comparison with other derivatives. The decrease in band gap in SeDPP-Hex can be rationalized by correlating the effect of selenium in lowering the LUMO energy level.[50] Moreover, decrease in aromaticity[51] and increase in quinoidal character in selenophene derivative also influence the reduction of the band-gap as reported by Bendikov and co-workers.[46] Secondly, TDPP-Hex and SeDPP-Hex clearly exhibit vibronic feature in the visible region representative of low energy transition. However, this feature was not observed for PDPP-Hex. The maxima of the low energy band appeared at ~470 nm for PDPP-Hex, but dual peaks were observed at ~510 nm, ~550 nm for TDPP-Hex and ~525 nm, ~562 nm for SeDPP-Hex.

To understand the variation in the spectral behavior, concentration dependent study was carried out on TDPP-Hex and SeDPP-Hex in toluene. Upon decreasing concentration of DPP derivatives from $27x10^{-6}$ to $7x10^{-7}$ M, both TDPP-Hex and SeDPP-Hex exhibit dual band vibronic features which rules out any aggregation in solution (Figure S7, ESI$^{\dagger}$). However, de-convolution of the low energy band of PDPP-Hex indicates that this band was also composed of two bands with peak maxima at ~460 nm and ~488 nm (Figure S5, ESI$^{\dagger}$). Nevertheless, the molar absorption coefficient steadily increases on moving from PDPP-Hex to TDPP-Hex to SeDPP-Hex. This trend suggests that orbital overlap between donor and acceptor group improves due to integration of chalcogen atom in the donor unit. Due to lesser electronegativity of selenium (2.55) as compared to sulfur (2.58) and lower aromaticity of selenophene than the thiophene, selenophene ring acts as a stronger donor group in comparison with thiophene,[51] leading to the higher stabilization of excited state. In addition, contribution of 'd' orbitals in the charge delocalization is anticipated to be higher in case of selenium as compared to sulfur due to bigger and diffused 'd' orbital of selenium. This clearly supports the highest absorption coefficient for SeDPP-Hex among three DPP derivatives.

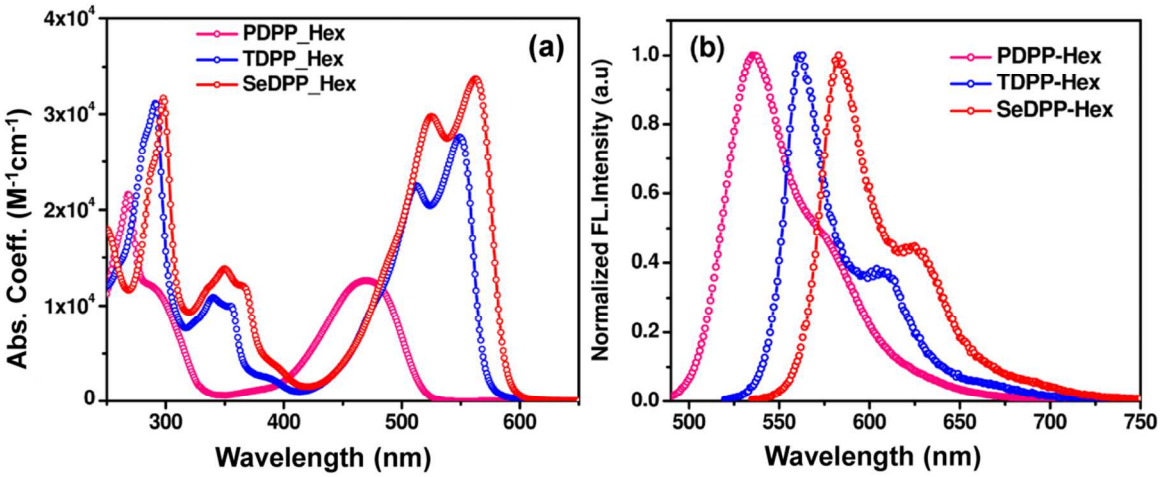


**Figure 1:** Absorption (a) and the emission spectra (b) of the three DPP molecules in toluene.

The emission spectra (Figure 1b) of three DPP derivatives have close resemblance in their spectral appearance with complementary dual band features. The compound PDPP-Hex also exhibits the dual band emission but was found to be less eminent in comparison with TDPP-Hex and SeDPP-Hex. Similar to the absorption spectra, the fluorescence spectra also showed bathochromic shift from PDPP-Hex to SeDPP-Hex with emission maxima at ~535 nm, ~560 nm and ~580 nm for PDPP-Hex, TDPP-Hex and SeDPP-Hex, respectively. The least Stokes shift was observed for TDPP-Hex (0.04 eV) and highest was obtained for PDPP-Hex (0.32 eV). The pertinent data of Stokes shift is summarized in Table 1. The observed less Stokes shift for TDPP-Hex implies that maximum rigidity is attained in the molecular backbone. Fluorescence quantum yield measurements reveal that PDPP-Hex exhibited high photo-luminescence quantum yield (PLQY) of 85% while TDPP-Hex and SeDPP-Hex show 79% and 66% respectively (Figure 2b). The gradual decrease of fluorescence quantum yield can be attributed to the heavy atom effect of sulfur and selenium which facilitates the inter-system crossing rates.[52] The fluorescence lifetime ($\tau_F$) for PDPP-Hex and TDPP-Hex exhibits mono exponential decay pattern while SeDPP-Hex demonstrates bi-exponential decay profile, as shown in Figure 2a. The lifetime systematically decreases from PDPP-Hex (~6.8 ns) to SeDPP-Hex (~5.5 ns, together with a species of 1.2 ns having amplitude of 14%) with the intermediate lifetime for TDPP-Hex (~6.2 ns).

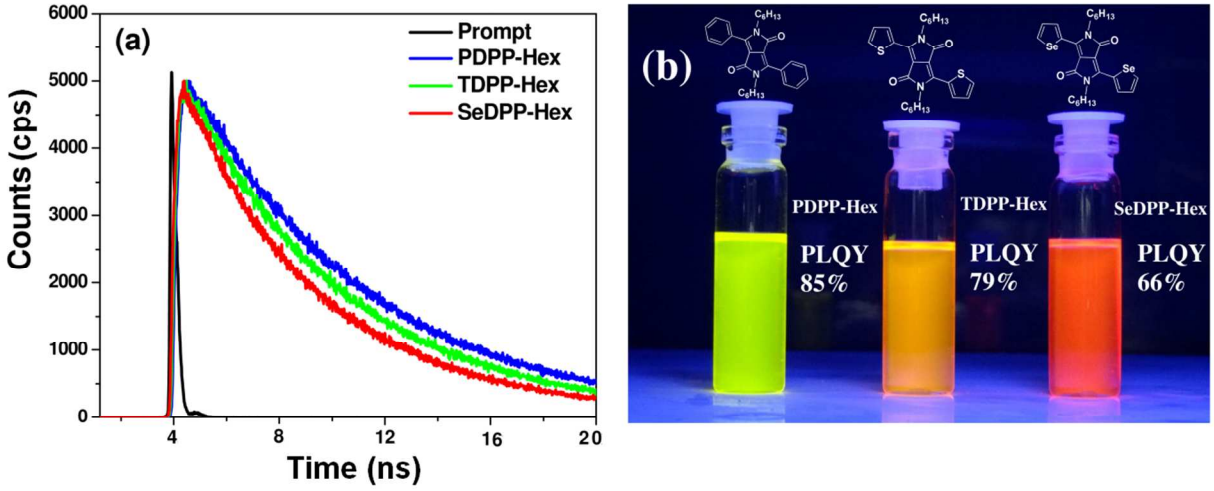


**Figure 2:** (a) Fluorescence lifetime decay pattern of DPP derivatives varied with different donor groups. (b) Photograph was taken to show the variation in the emitting behavior of three different DPP derivatives under illumination of UV light (~365nm).

**Table 1:** Summary on photophysical data of three DPP derivatives varied with different donor units.

| compound | $\lambda_{abs}$ (nm) | $\varepsilon_{max}$ ($M^{-1}cm^{-1}$) | $\lambda_{em}$ (nm) | Stokes Shift (eV) | Electrochemical# | | | DFT* |
|---|---|---|---|---|---|---|---|---|
| | | | | | HOMO (eV) | LUMO (eV) | $\Delta E_g$ (eV) | $\Delta E_g$ (eV) |
| PDPP-Hex | 480 | 12600 | 535,575 | 0.32 | -5.71 | -3.08 | 2.63 | 2.85 |
| TDPP-Hex | 510,550 | 27600 | 562,606 | 0.04 | -5.56 | -3.10 | 2.46 | 2.44 |
| SeDPP-Hex | 525,562 | 33600 | 583,625 | 0.07 | -5.49 | -3.20 | 2.29 | 2.40 |

# The data obtained from cyclic voltammetry with reference to Ag/AgCl electrode and Ferrocene/ferrocenium ($Fc/Fc^+$) couple as standard.
* The values obtained from difference between the HOMO and LUMO energy levels optimized at B3LYP/6-31g* basis set.

### 3.2 DFT and TD-DFT calculations

Density Functional Theory (DFT) calculations were performed to reveal the optimized geometry of the ground state, electron density distribution and the energy associated with the frontier molecular orbitals. The B3LYP function with 6-31g* basis set was employed for the geometry optimization and time dependent density functional (TD-DFT) calculations in Gaussian 03 suite programme. The optimized geometries and electron density distribution in HOMO and LUMO of three DPP derivatives are shown in Figure 3. The optimized geometry of TDPP-Hex and SeDPP-Hex exhibit the *trans*-orientation of the heterocycle with respect to each other. The donor and the acceptor groups lie in the same plane with small variations in torsional angle (~1° and ~2° for TDPP-Hex and SeDPP-Hex respectively) which improves 'p' orbitals overlap over the molecular backbone. But PDPP-Hex exhibits high torsional angle (~36°) between lactam and phenyl ring which results in poorer overlap of the 'p' orbitals reflecting in the electron distribution in its frontier orbitals.

In HOMO, the electron density over the phenyl ring is almost negligible and mainly localized over the lactam ring indicating weak electronic coupling between donor and acceptor groups. However, the LUMO is evenly distributed over the donor as well as on the acceptor moieties. The distribution of electron density appears different with the substitution of thiophene/selenophene as a donor in place of phenyl. The planarity of the donor and acceptor moieties improves the delocalization of wave-function and we observe uniform distribution of electron density in HOMO as well as in LUMO for both TDPP-Hex and SeDPP-Hex. The inter ring (in between donor and acceptor group) C-C bond length also decreases with decrease in aromatic resonance energy of the donor moiety. The C-C bond length varies in the order, PDPP-Hex (1.46 Å) > TDPP-Hex (1.44 Å) > SeDPP-Hex (1.43 Å) implying gradual increase in quinoidal character of the C-C bond from PDPP-Hex to SeDPP-Hex. The optimized geometries and electron density distribution in HOMO and LUMO along with the energies are shown in Figure 3.

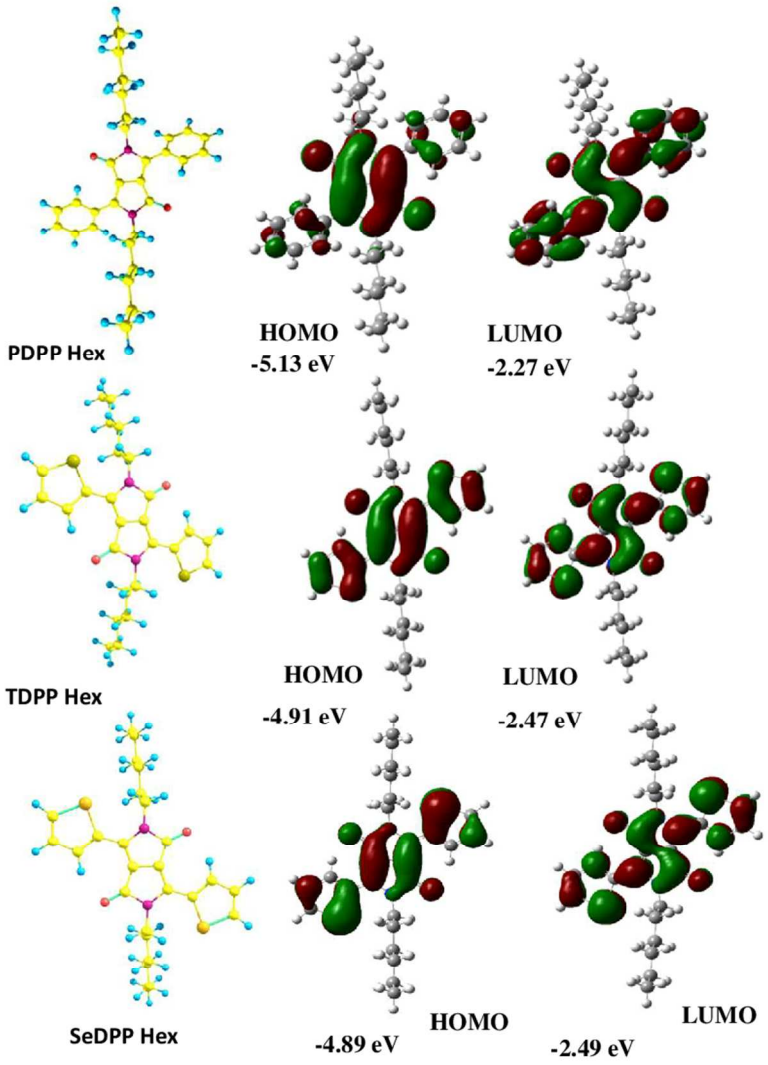


**Figure 3:** Energy minimized ground state geometry and corresponding electron distribution in the frontier molecular orbitals of three DPP derivatives.

PDPP-Hex showed the deepest lying HOMO energy level (-5.13 eV) whereas the other two derivatives containing chalcogen atoms increase the HOMO energy due to strong electron donating strength. On the other hand, the LUMO energy is decreased with inclusion of chalcogen atom in DPP. This data suggests that low ionization potential of selenium than sulfur causes the shift in LUMO energy.[50] The HOMO-LUMO gap was found to decrease in the order of PDPP-Hex (2.85 eV) > TDPP-Hex (2.44 eV) > SeDPP-Hex (2.40 eV).

**Table 2:** Summary of excited state electronic transitions obtained from TD-DFT calculations

| Compounds | Dominant Contribution (%) | Absorption (nm) | Energy (eV) | Oscillator strength *(f)* | Dipole Moment (D) |
|---|---|---|---|---|---|
| **PDPP-Hex** | H → L (70.7%) | 456.69 | 2.71 | 0.4006 | 0.46 |
| | H-3→ L (51.8%) | 324.54 | 3.82 | 0.0314 | |
| | H-6→ L (62.0%) | 301.34 | 4.11 | 0.0015 | |
| **TDPP-Hex** | H → L (58.6%) | 517.92 | 2.39 | 0.4882 | 0.48 |
| | H-2 → L (53.05%) | 325.14 | 3.81 | 0.1956 | |
| | H-7 → L (57.21%) | 319.92 | 3.87 | 0.0906 | |
| **SeDPP-Hex** | H → L (71.2%) | 527.49 | 2.35 | 0.5081 | 0.53 |
| | H-4 → L (63.23%) | 332.05 | 3.73 | 0.1149 | |
| | H-2 → L (63.23%) | 325.76 | 3.80 | 0.1596 | |

The TD-DFT calculations were also performed to ascertain the orbitals involved in the dominant excited state electronic transitions; their corresponding energies and oscillator strength have been summarized in Table 2. For all three DPP molecules, the low energy band constitutes with the transition from HOMO→LUMO. From Table 2, we found that the oscillator strength gradually increases from PDPP-Hex to TDPP-Hex to SeDPP-Hex due to enhancement in the electronic coupling between donor and acceptor moieties corroborating our finding from optical spectroscopy. By changing the donor moiety from phenyl to thiophene to selenophene, the low energy transition shifts from ~457 nm to ~517 nm to ~527 nm. The simulated absorption spectra of these three DPP molecules (Figure S6, ESI$^{\dagger}$) follow the same trend as it was observed in experimental results. The molar absorption coefficient increases with gradual bathochromic shift as we move from PDPP-Hex to TDPP-Hex to SeDPP-Hex. The variations in the absorption maxima between theoretical calculations and experimental observations can be attributed to the different parameters e.g. influence of bulk state and solvent molecules which are not accounted for the TD-DFT calculations.

### 3.3 Electrochemical Properties

The electrochemical properties of three derivatives were investigated by cyclic voltammetry and voltammograms are shown in Figure 4. All the DPP derivatives (**PDPP-Hex, TDPP-Hex and SeDPP-Hex**) exhibit low lying HOMO energy level and among them PDPP-Hex demonstrated the deepest level of HOMO energy, calculated from its peak position of oxidation potential. PDPP-Hex exhibits an irreversible oxidation and reduction peak while for other two derivatives the oxidation and reduction are quasi-reversible in nature. This indicates the influence of heteroatom (sulfur and selenium) on DPP derivatives to stabilize the radical cation and/or radical anion during redox reaction. The HOMO and LUMO energy values are summarized in Table 1. The LUMO energies calculated from the reduction potential clearly indicate that incorporation of selenium in DPP has pronounced effect in reducing the LUMO energy level. The difference between LUMO energy levels of TDPP-Hex and SeDPP-Hex is more pronounced than the value obtained from DFT calculations. The observation of low lying LUMO energy of SeDPP-Hex has great importance in developing new stable *n*-type materials. This effect was further supported by the recent observation of *n*-type character for polymers incorporated with selenium in the molecular backbone.[53] The LUMO of PDPP-Hex was found to be of similar energy as TDPP-Hex. The band gap calculated from electrochemical measurement was found to be similar with the optical band gap.

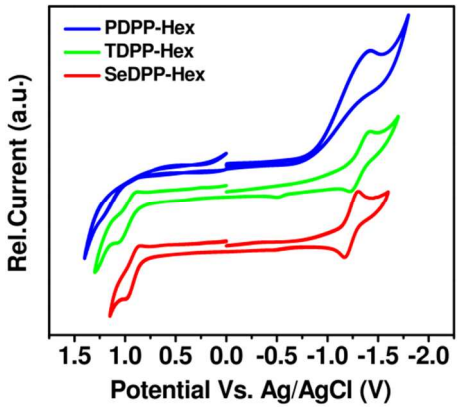


**Figure 4:** Cyclic voltammograms of three DPP derivatives varied with different donor units.

### 3.4 Crystal Structure and Molecular Arrangement

Single crystal X-ray diffraction studies were performed to investigate crystal structure, molecular interaction and solid state packing. Single crystals of all three DPP molecules were grown from hexane: acetone (6:4) solvents combination by slow evaporation method. The compounds PDPP-Hex and TDPP-Hex form sharp and long needle like crystals while SeDPP-Hex forms tiny crystals. The three derivatives crystallized in monoclinic space group $P2_1/c$ with z=2. Figure 5 shows the molecular arrangements of the DPP derivatives along tilted c-axis. It can be seen that all three DPP derivatives were arranged in herringbone fashion. Like TDPP-Hex, SeDPP-Hex also exhibits weak π-π stacking interaction as two neighboring molecules are slipped away from each other.

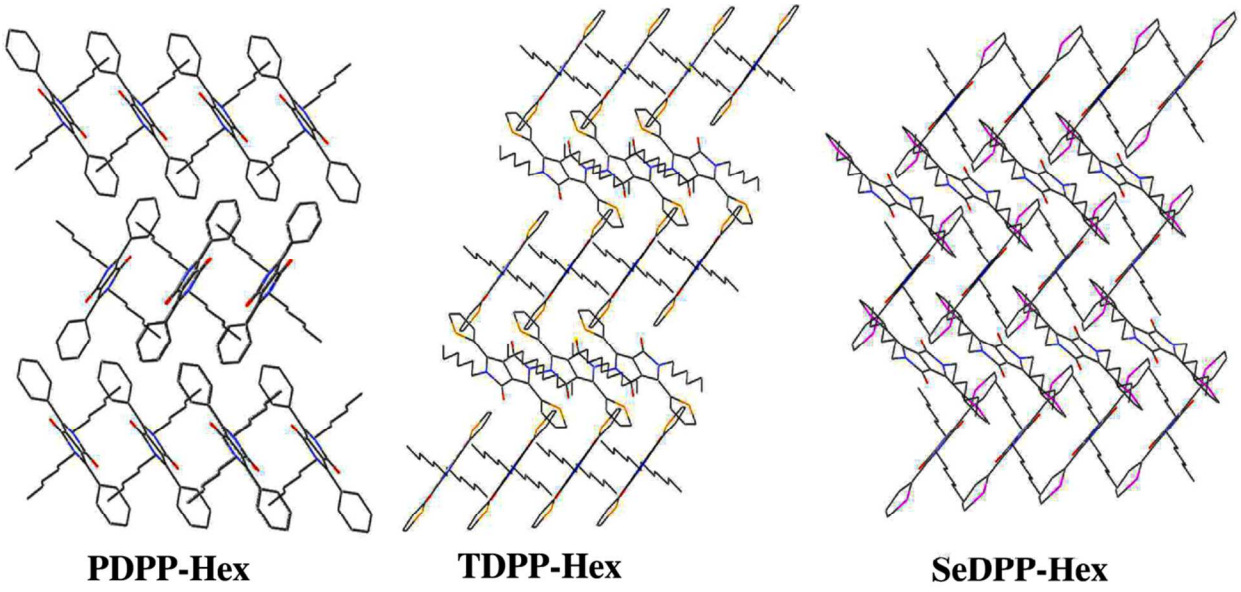


**Figure 5:** Molecular arrangements of three DPP derivatives varied with different donor units.

The π-π stacking distance of ~5.39 Å and ~5.52 Å was obtained between two heterocyclic rings for TDPP-Hex and SeDPP-Hex, respectively. Due to such slipped stacking, the heterocycle e.g. thiophene or selenophene overlaps with the lactam ring of the nearby molecule, as shown in Figure 6. Similar kind of intermolecular interaction between electron rich donor and electron deficient acceptor unit has been observed in other D-A system.[54] As a result, the distance between lactam ring of DPP core and nearby heterocycle appeared to be shorter and the measured π-π stacking distances were found to be 3.61 Å for both molecules. On the other hand,

the distance between nitrogen atom of the lactam ring and the corresponding chalcogen atom was found to be 3.89 Å and 3.98 Å for TDPP-Hex and SeDPP-Hex, respectively. However, the Se···O bond distance (4.14 Å) was shorter than S···O bond distance (4.21 Å) though the van der Waals radius of selenium (1.90 Å) is larger than that of sulfur atom (1.80 Å). As observed in theoretical calculations, the non-bonding interaction between N and S, involving 'd' orbitals of sulfur can operate even at the distance of 3.8 Å.[55] Based on these observations, we speculate that very weak non-bonding interactions are operational for both TDPP-Hex and SeDPP-Hex in crystal lattice and the amplitude of such interaction is anticipated to be higher in case of Se···N in comparison with S···N. In addition to π-π interaction, we have also observed the presence of C-H···O hydrogen bonding interaction between C=O of lactam ring and C-H of heterocycle with the bond length of 2.71 Å and 2.67 Å for thiophene and selenophene analogues, respectively. Furthermore, the torsional angle between donor (selenophene and thiophene) and acceptor (lactam) ring in SeDPP-Hex increases marginally to 12° in comparison with TDPP-Hex (9°) (Figure S8, ESI†). Since, the planarity between donor and acceptor unit remained almost same for TDPP-Hex and SeDPP-Hex, the electronic coupling between donor and acceptor moiety does not change significantly to influence the charge delocalization over the molecular backbone. In contrast, PDPP-Hex exhibits quite different packing arrangement in the crystal lattice and the packing pattern resembles like orthorhombic system with small deviation from ideal orthogonality of the unit cell α=γ=90°, β=90.06°. PDPP-Hex molecule also exhibits slipped weak π-π interaction with the distance of 5.54 Å between two phenyl rings. The high torsional angle of 33° (Figure S8, ESI†) between phenyl and lactam ring limits the orbital overlap among donor and acceptor units resulting in poor intramolecular interactions. The large torsional angle originates from the steric repulsion between *ortho* hydrogen atom of phenyl ring and nearby hydrogen atom of alkyl chain placed on the nitrogen atom of the lactam unit. The detrimental effect of torsional angle renders the lower absorption co-efficient in PDPP-Hex as compared to other derivatives. The variations in inter-ring C-C as well as C-N bond length for three DPP based molecules are listed in Table S1, ESI†. But some significant C-X (X=S or Se) bond length alteration was found between two chalcogen analogues. It can be seen that, the bond length increases with incorporation of selenium in place of sulfur due to bigger atomic size of selenium (van der Waals radius, r=1.9 Å) in comparison with sulfur (r=1.8 Å).

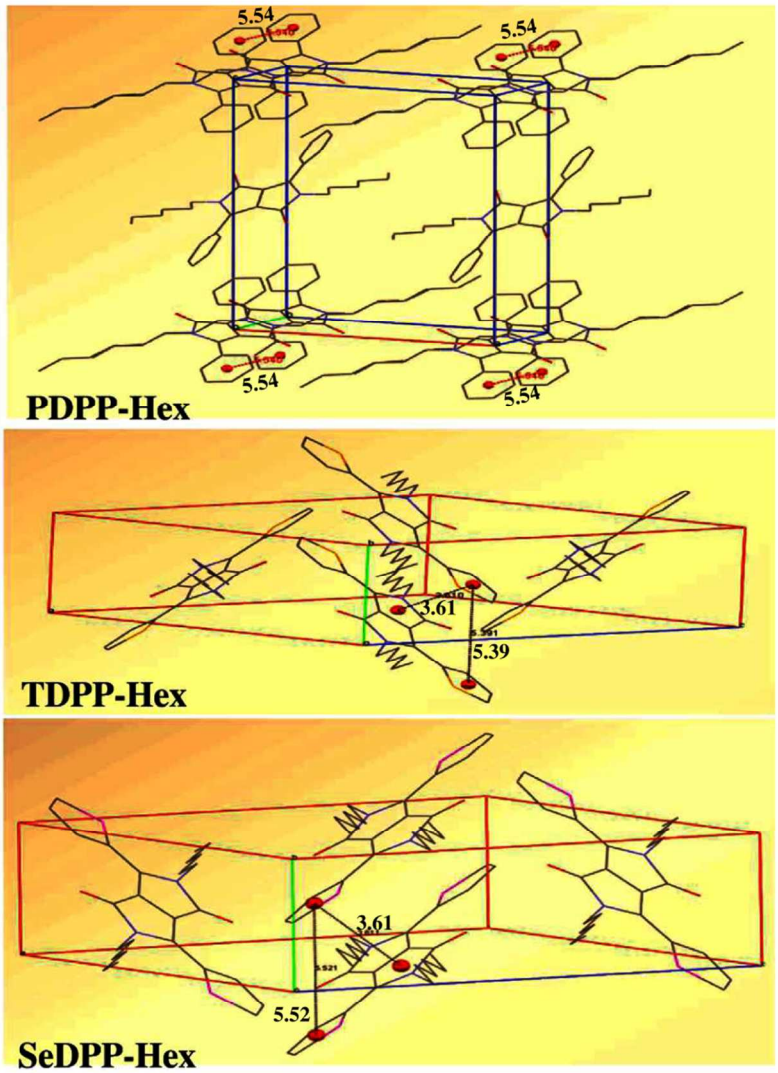


**Figure 6:** Unit cell packing diagram of DPP derivatives.

### 3.4 Thin Film X-ray Analysis and Microscopy

Thin films of all three DPP derivatives were fabricated on silicon substrates by sublimation technique. The high crystallinity of these materials is reflected in their X-ray diffraction pattern. Figure 7 shows thin film X-ray diffractograms of these three DPP based derivatives. Only few selected diffraction peaks appeared in the diffractogram indicating the presence of highly oriented crystallites. Except TDPP-Hex, the other two molecules showed four peaks within 2θ= 3-30°. The diffraction peaks with their corresponding *'d'* values of these three molecules are summarized in Table 3. As shown in Figure 7, that the '*d*' spacing of (100) gradually increases

from PDPP-Hex to TDPP-Hex to SeDPP-Hex. The nature of packing pattern for TDPP-Hex and SeDPP-Hex was quite similar to the simulated X-ray diffraction pattern obtained from the single crystal diffraction study. The enhancement in '*d*' spacing can be attributed to the bigger size of selenium as compared to the size of sulfur. The '*d*' spacing of 3.6 Å matches well with the π-π stacking distance as observed in single crystal X-ray diffraction pattern.

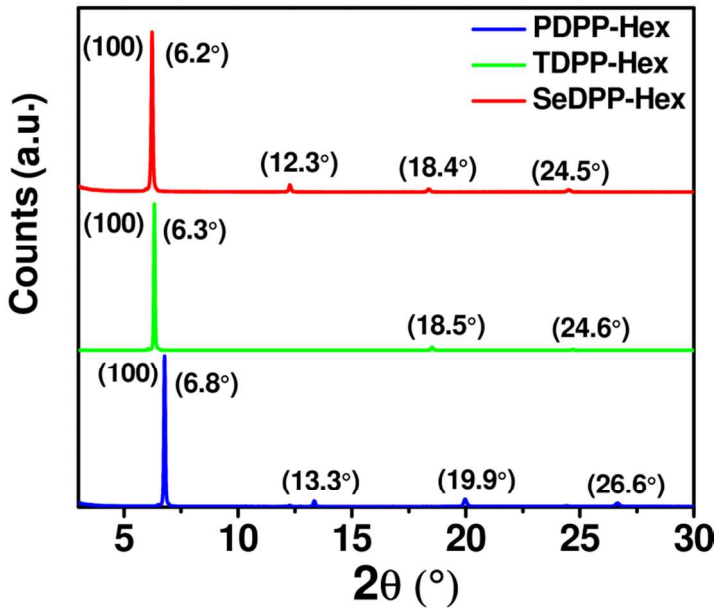


**Figure 7:** Thin film X-ray diffractogram of three DPP derivatives deposited on Si substrates.

**Table 3:** Summary of powder X-ray diffraction peaks and its corresponding '*d*' spacing.

| | $2\theta_1$ ($d_1$) | $2\theta_2$ ($d_2$) | $2\theta_3$ ($d_3$) | $2\theta_4$ ($d_4$) |
|---|---|---|---|---|
| **PDPP-Hex** | 6.8° (13.0 Å) | 13.3° (6.4 Å) | 19.9° (4.4 Å) | 26.6° (3.3 Å) |
| **TDPP-Hex** | 6.3° (14.1 Å) | ….. | 18.5° (4.8 Å) | 24.6° (3.6 Å) |
| **SeDPP-Hex** | 6.2° (14.8 Å) | 12.3° (7.2 Å) | 18.4° (4.8 Å) | 24.5° (3.6 Å) |

Further, the formation of self-assembly was investigated by high resolution transmission electron microscopy (HR-TEM). The dilute solutions of DPP derivatives in toluene were drop casted on carbon coated copper grid and observed under TEM. It was found that they aggregate without any proper structural features. But the aggregates were found to be highly polycrystalline in nature. The aggregation phenomenon of these DPP based molecules was governed by the nature

of the substrates which influence the self-assembly of the molecules. From HRTEM, we were able to measure the '*d*' spacing for these three molecules. For PDPP-Hex, we observe the diffraction pattern with varied '*d*' values. On the other hand, TDPP-Hex and SeDPP-Hex exhibit two distinct '*d*' spacings and the values are summarized in Table S2, ESI†. For PDPP-Hex the '*d*' spacing of 10.4 Å was predominant as compared to the other '*d*' values. The calculated '*d*' spacings were very close to the distances between S···S and Se···Se in TDPP-Hex and SeDPP-Hex, as observed in single crystal diffraction data (Figure S9,ESI†). We believe that crystal planes with higher contrast in HRTEM image for TDPP-Hex and SeDPP-Hex might contain chalcogen atoms, since they are heavier as compared to the other elements present in these two molecules.

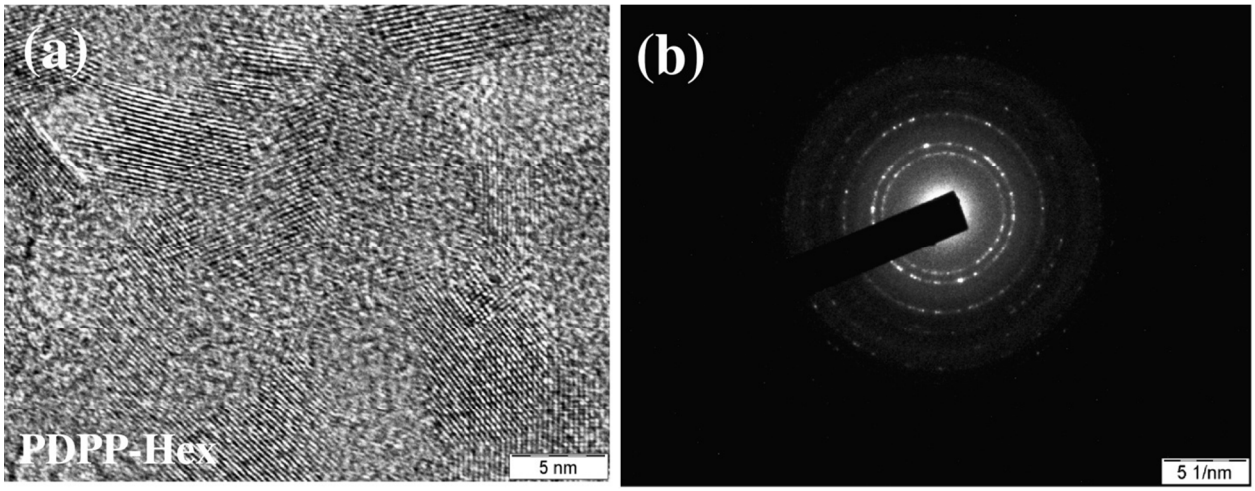


**Figure 8:** HR-TEM (a) and SAED (b) pattern of PDPP-Hex

### 3.5 Thermal properties

The thermal transitions and enthalpies of the DPP based derivatives were obtained by differential scanning calorimetry (DSC). All three DPP derivatives exhibit single reversible melting and crystallization peak during heating and cooling processes. Among three molecules, TDPP-Hex demonstrated highest (173 °C) and PDPP-Hex showed the lowest (134 °C) melting temperature and SeDPP-Hex exhibits melting temperature at 140 °C (Figure 9). From DSC experiments, we observe that thermal hysteresis gradually diminishes as we move from PDPP-Hex to TDPP-Hex to SeDPP-Hex. This implies the disorder to order transition in SeDPP-Hex to be enthalpically more favorable as compared to the other two DPP derivatives. We apprehend that due to

incorporation of heavier atom (Se) in molecular architecture, the melting point decreases because of higher thermal motion as a result of size restrain but higher polarisability of selenium atom assists to reorganize the molecules to crystallize with least thermal hysteresis.

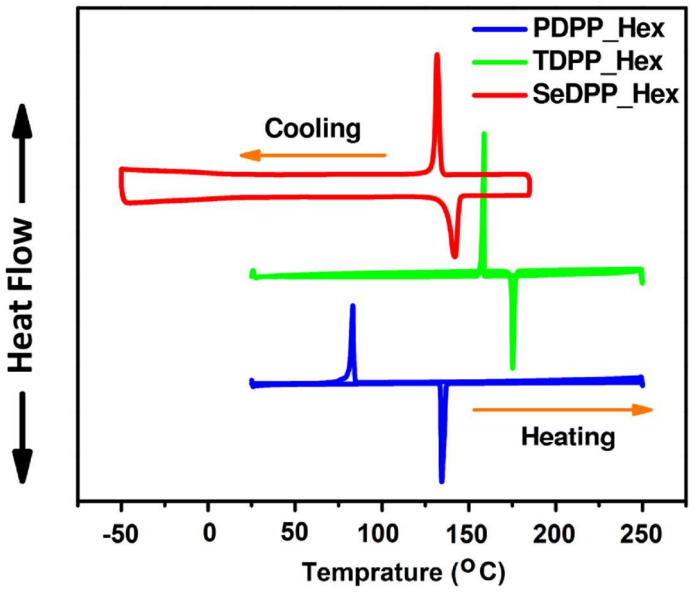


**Figure 9:** DSC thermogram of three DPP derivatives under nitrogen flow.

## 4. Conclusions

In summary, the present results highlight the importance of donor group in determining solid state and photophysical properties of DPP. The influences of donor unit on solid state packing arrangement of DPP were studied by single crystal X-ray diffraction. The detrimental effect of torsional angle in PDPP-Hex due to steric repulsion between the *ortho* hydrogen atom of phenyl ring and nearby hydrogen atom of alkyl chain renders weak intramolecular interaction. The presence of slipped stacking interaction in TDPP-Hex and SeDPP-hex stabilizes efficient π-π overlap of donor (thiophene and selenophene) to acceptor DPP unit. The significant C-X (X=S, Se) bond alterations and variation in Se···O and S···O distances indicate SeDPP-Hex has efficient diffusion with high polarizability. Variation in donor groups strongly influences the optical band gap and molar absorption co-efficient. The electrochemical study reveals that the presence of chalcogen atom stabilizes the formation of radical ions during the redox processes. Incorporation of selenium in the molecular architecture exhibits pronounced effect in stabilizing the LUMO energy levels. This report provides an insight into the role of chalcogen and torsional angle in determining the solid

state and photophysical properties of DPP. Such apprehension will have an important contribution to the development of new *n*-type materials for optoelectronic devices.

## 5. Acknowledgements

We would like to thank Mr. K. Durga Prasad for helping us in recording and analyzing the X-ray crystal data. Joydeep Dhar greatly acknowledges the Council of Scientific and Industrial Research (CSIR) for senior research fellowship (SRF). The authors are grateful to Dr. Deepak Kumar for his help in electrochemical measurements and Catherine Kanimozhi for useful discussions. S.P. thanks the Department of Science and Technology, New Delhi for financial support through India-Israel research project No. DST/INT/ISR/P-6/2011 and the Science and Engineering Research Board through a project No.SR/S1/PC-40/2010.

## 6. References

1. J. G. Mei, Y. Diao, A. L. Appleton, L. Fang and Z. N. Bao, *J. Am. Chem. Soc.*, 2013, **135**, 6724-6746.
2. B. Walker, C. Kim and T. Q. Nguyen, *Chem. Mater.*, 2011, **23**, 470-482.
3. Y. Z. Lin, Y. F. Li and X. W. Zhan, *Chem. Soc. Rev.*, 2012, **41**, 4245-4272.
4. A. W. Hains, Z. Q. Liang, M. A. Woodhouse and B. A. Gregg, *Chem. Rev.*, 2010, **110**, 6689-6735.
5. E. E. Havinga, W. Tenhoeve and H. Wynberg, *Polym. Bull.*, 1992, **29**, 119-126.
6. E. E. Havinga, W. Tenhoeve and H. Wynberg, *Synth. Met.*, 1993, **55**, 299-306.
7. C. Kitamura, S. Tanaka and Y. Yamashita, *Chem. Mater.*, 1996, **8**, 570-578.
8. S. Roquet, A. Cravino, P. Leriche, O. Aleveque, P. Frere and J. Roncali, *J. Am. Chem. Soc.*, 2006, **128**, 3459-3466.
9. C. Kanimozhi, N. Yaacobi-Gross, K. W. Chou, A. Amassian, T. D. Anthopoulos and S. Patil, *J. Am. Chem. Soc.*, 2012, **134**, 16532-16535.
10. Y. J. Cheng, S. H. Yang and C. S. Hsu, *Chem. Rev.*, 2009, **109**, 5868-5923.
11. O. Gidron, N. Varsano, L. J. W. Shimon, G. Leitus and M. Bendikov, *Chem. Commun.*, 2013, **49**, 6256-6258.
12. A. A. B. Alghamdi, D. C. Watters, H. N. Yi, S. Al-Faifi, M. S. Almeataq, D. Coles, J. Kingsley, D. G. Lidzey and A. Iraqi, *J. Mater. Chem. A*, 2013, **1**, 5165-5171.
13. X. R. Zhang, L. J. Richter, D. M. DeLongchamp, R. J. Kline, M. R. Hammond, I. McCulloch, M. Heeney, R. S. Ashraf, J. N. Smith, T. D. Anthopoulos, B. Schroeder, Y. H. Geerts, D. A. Fischer and M. F. Toney, *J. Am. Chem. Soc.*, 2011, **133**, 15073-15084.
14. A. Mishra and P. Bauerle, *Angew. Chem.-Int. Edit.*, 2012, **51**, 2020-2067.
15. J. Li, K. H. Ong, S. L. Lim, G. M. Ng, H. S. Tan and Z. K. Chen, *Chem. Commun.*, 2011, **47**, 9480-9482.
16. S. Loser, C. J. Bruns, H. Miyauchi, R. P. Ortiz, A. Facchetti, S. I. Stupp and T. J. Marks, *J. Am. Chem. Soc.*, 2011, **133**, 8142-8145.
17. M. A. Naik and S. Patil, *J. Polym. Sci., Part a: Polym. Chem.*, 2013, **51**, 4241-4260.
18. S. Y. Qu and H. Tian, *Chem. Commun.*, 2012, **48**, 3039-3051.

19. L. T. Dou, J. B. You, J. Yang, C. C. Chen, Y. J. He, S. Murase, T. Moriarty, K. Emery, G. Li and Y. Yang, *Nat. Photonics*, 2012, **6**, 180-185.
20. Y. N. Li, P. Sonar, L. Murphy and W. Hong, *Energy Environ. Sci.*, 2013, **6**, 1684-1710.
21. Q. T. Zhang and J. M. Tour, *J. Am. Chem. Soc.*, 1998, **120**, 5355-5362.
22. C. B. Nielsen, M. Turbiez and I. McCulloch, *Adv. Mater.*, 2013, **25**, 1859-1880.
23. L. T. Dou, W. H. Chang, J. Gao, C. C. Chen, J. B. You and Y. Yang, *Adv. Mater.*, 2013, **25**, 825-831.
24. W. W. Li, A. Furlan, K. H. Hendriks, M. M. Wienk and R. A. J. Janssen, *J. Am. Chem. Soc.*, 2013, **135**, 5529-5532.
25. J. Lee, A. R. Han, H. Yu, T. J. Shin, C. Yang and J. H. Oh, *J. Am. Chem. Soc.*, 2013, **135**, 9540-9547.
26. I. Kang, H. J. Yun, D. S. Chung, S. K. Kwon and Y. H. Kim, *J. Am. Chem. Soc.*, 2013, **135**, 14896-14899.
27. I. Kang, T. K. An, J. A. Hong, H. J. Yun, R. Kim, D. S. Chung, C. E. Park, Y. H. Kim and S. K. Kwon, *Adv. Mater.*, 2013, **25**, 524-528.
28. K. Tandy, G. K. Dutta, Y. L. Zhang, N. Venkatramaiah, M. Aljada, P. L. Burn, P. Meredith, E. B. Namdas and S. Patil, *Org. Electron.*, 2012, **13**, 1981-1988.
29. C. Kanimozhi, P. Balraju, G. D. Sharma and S. Patil, *J. Phys. Chem. C*, 2010, **114**, 3287-3291.
30. M. A. Naik, N. Venkatramaiah, C. Kanimozhi and S. Patil, *J. Phys. Chem. C*, 2012, **116**, 26128-26137.
31. P. Sonar, S. P. Singh, E. L. Williams, Y. N. Li, M. S. Soh and A. Dodabalapur, *J. Mater. Chem.*, 2012, **22**, 4425-4435.
32. P. Sonar, J. M. Zhuo, L. H. Zhao, K. M. Lim, J. H. Chen, A. J. Rondinone, S. P. Singh, L. L. Chua, P. K. H. Ho and A. Dodabalapur, *J. Mater. Chem.*, 2012, **22**, 17284-17292.
33. L. Biniek, B. C. Schroeder, C. B. Nielsen and I. McCulloch, *J. Mater. Chem.*, 2012, **22**, 14803-14813.
34. P. Sonar, S. P. Singh, Y. Li, M. S. Soh and A. Dodabalapur, *Adv. Mater.*, 2010, **22**, 5409-5413.
35. M. Shahid, T. McCarthy-Ward, J. Labram, S. Rossbauer, E. B. Domingo, S. E. Watkins, N. Stingelin, T. D. Anthopoulos and M. Heeney, *Chem. Sci.*, 2012, **3**, 181-185.
36. A. B. Tamayo, B. Walker and T. Q. Nguyen, *J. Phys. Chem. C*, 2008, **112**, 11545-11551.
37. X. D. Dang, A. B. Tamayo, J. Seo, C. V. Hoven, B. Walker and T. Q. Nguyen, *Adv. Funct. Mater.*, 2010, **20**, 3314-3321.
38. H. Bronstein, Z. Y. Chen, R. S. Ashraf, W. M. Zhang, J. P. Du, J. R. Durrant, P. S. Tuladhar, K. Song, S. E. Watkins, Y. Geerts, M. M. Wienk, R. A. J. Janssen, T. Anthopoulos, H. Sirringhaus, M. Heeney and I. McCulloch, *J. Am. Chem. Soc.*, 2011, **133**, 3272-3275.
39. I. McCulloch, M. Heeney, C. Bailey, K. Genevicius, I. Macdonald, M. Shkunov, D. Sparrowe, S. Tierney, R. Wagner, W. M. Zhang, M. L. Chabinyc, R. J. Kline, M. D. McGehee and M. F. Toney, *Nat. Mater.*, 2006, **5**, 328-333.
40. H. Bronstein, E. Collado-Fregoso, A. Hadipour, Y. W. Soon, Z. Huang, S. D. Dimitrov, R. S. Ashraf, B. P. Rand, P. S. Tuladhar, S. E. Watkins, I. Meager, J. R. Durrant and I. McCulloch, *Adv. Funct. Mater.*, 2013, **DOI: 10.1002/adfm.201300287**.
41. J. C. Bijleveld, B. P. Karsten, S. G. J. Mathijssen, M. M. Wienk, D. M. de Leeuw and R. A. J. Janssen, *J. Mater. Chem.*, 2011, **21**, 1600-1606.

42. M. Shahid, R. S. Ashraf, Z. G. Huang, A. J. Kronemeijer, T. McCarthy-Ward, I. McCulloch, J. R. Durrant, H. Sirringhaus and M. Heeney, *J. Mater. Chem.*, 2012, **22**, 12817-12823.
43. A. J. Kronemeijer, E. Gili, M. Shahid, J. Rivnay, A. Salleo, M. Heeney and H. Sirringhaus, *Adv. Mater.*, 2012, **24**, 1558-1565.
44. E. Poverenov, Y. Sheynin, N. Zamoshchik, A. Patra, G. Leitus, I. F. Perepichka and M. Bendikov, *J. Mater. Chem.*, 2012, **22**, 14645-14655.
45. A. Patra and M. Bendikov, *J. Mater. Chem.*, 2010, **20**, 422-433.
46. S. S. Zade, N. Zamoshchik and M. Bendikov, *Chem.- Eur. J.*, 2009, **15**, 8613-8624.
47. C. Bleiholder, D. B. Werz, H. Koppel and R. Gleiter, *J. Am. Chem. Soc.*, 2006, **128**, 2666-2674.
48. A. R. Rabindranath, Y. Zhu, I. Heim and B. Tieke, *Macromolecules*, 2006, **39**, 8250-8256.
49. G. Lohaus, *Chem. Ber.*, 1967, **100**, 2719-2729.
50. H. O. Villar, P. Otto, M. Dupuis and J. Ladik, *Synth. Met.*, 1993, **59**, 97-110.
51. Fringuel.F, G. Marino, A. Taticchi and Grandoli.G, *J. Chem. Soc., Perkin Trans. 2*, 1974, 332-337.
52. R. Q. Yang, R. Y. Tian, Q. Hou, Z. Yong, Y. F. Li, Y. Wei, Z. Chi and C. Yong, *J. Polym. Sci., Part a: Polym. Chem.*, 2005, **43**, 823-836.
53. H. W. Lin, W. Y. Lee and W. C. Chen, *J. Mater. Chem.*, 2012, **22**, 2120-2128.
54. H. Y. Liu, H. Jia, L. F. Wang, Y. S. Wu, C. L. Zhan, H. B. Fu and J. N. Yao, *Phys. Chem. Chem. Phys.*, 2012, **14**, 14262-14269.
55. N. E. Jackson, B. M. Savoie, K. L. Kohlstedt, M. O. de la Cruz, G. C. Schatz, L. X. Chen and M. A. Ratner, *J. Am. Chem. Soc.*, 2013, **135**, 10475-10483.